Function of ERphagy receptors is regulated via phosphorylation-dependent ubiquitination pathways

Rayene Berkane[1,2], Hung Ho-Xuan[1,2], Marius Glogger[3], Pablo Sanz Martinez[1,2], Sara Cano Franco[1,2], Thomas Juretschke[4], Alexis Gonzalez Cardenas[1], Tristan Glaesner[1], Petra Beli[4], Koraljka Husnjak[1], Volker Dötsch[5], Paolo Grumati[6,7], Mike Heilemann[3] and Alexandra Stolz[1,2]*

Affiliations:

[1] Institute of Biochemistry II (IBC2), Faculty of Medicine, Goethe University, Frankfurt am Main, Germany

[2] Buchmann Institute for Molecular Life Sciences (BMLS), Goethe University, Frankfurt am Main, Germany

[3] Institute of Physical and Theoretical Chemistry, Goethe University, Frankfurt am Main, Germany

[4] Institute of Molecular Biology, Mainz, Germany

[5] Institute of Biophysical Chemistry and Center for Biomolecular Magnetic Resonance, Goethe University, Frankfurt am Main, Germany

[6] Telethon Institute of Genetics and Medicine (TIGEM), Pozzuoli, Italy.

[7] Department of Clinical Medicine and Surgery, Federico II University, Naples, Italy

*Corresponding author

Keywords: endoplasmic reticulum, selective autophagy, FAM134B, FAM134C, lysosomal degradation, ER remodeling, ER fragmentation, ER homeostasis, stress response, ATM, ATR, CHEK1, CK2, mTOR, ubiquitination,

Abbreviations:

Akt: RAC-alpha serine/threonine-protein kinase

ATM: Ataxia-Telangiectasia Mutated

ATR: Ataxia-Telangiectasia and Rad3 related

Chk1: Checkpoint kinase1

CK2: Casein Kinase 2

CTRL: control

DOX: Doxycycline

E1: ubiquitin-activating enzyme

ER: Endoplasmic Reticulum

GABARAP: gamma aminobutyric acid receptor-associated protein

GFP: green fluorescent protein

HA: human infuenza hemmaglutinin

Ki: inhibition constant

LC3: MAP1LC3 microtubule-associated proteins 1A/1B light chain 3

LIR: LC3 interaction motif

PTMs: post-translational modifications

RFP: red fluorescent protein

RHD: Reticulon Homology Domain

WT: Wild type

Abstract

Selective autophagy of the ER (ERphagy) is an important regulator of ER remodeling and critical to maintain cellular homeostasis upon environmental changes. ERphagy receptors link the ER with autophagic membrane thus regulating ERphagy flux. We recently showed that members of the FAM134 family play overlapping and distinct roles during stress-induced ERphagy. Yet the mechanisms on how they are activated remain largely unknown. In this study we analyzed mTOR-mediated dynamic phosphorylation of FAM134 as a trigger of FAM134-driven ERphagy. An unbiased screen of kinase inhibitors revealed CK2 to be essential for FAM134B- and FAM134C-driven ERphagy upon mTOR inhibition. Identified dynamic phosphorylation sites on FAM134C in cells were fitting with predicted CK2 targeting sites, indicating a direct regulatory role of CK2 in FAM134-driven ERphagy. Using super-resolution microscopy, we showed that activity of CK2 is essential for the formation of high-density clusters of FAM134B and FAM134C. Consistently, FAM134B and FAM134C proteins carrying point mutations of selected Serin residues, within their reticulon homology domain, are unable to form high-density clusters. In addition, we provide evidence that the ubiquitination machinery is required for ERphagy and that FAM134B and FAM134C clustering is activated by phospho-dependent ubiquitination. Treatment with CK2 inhibitor SGC-CK2-1 prevents Torin1-induced ERphagy flux as well as ubiquitination of FAM134 proteins and consistently, treatment with E1 inhibitor suppresses Torin1-induced ERphagy flux. Therefore, we propose CK2 dependent phosphorylation of ERphagy receptors precedes ubiquitin-dependent ERphagy flux activation.

Introduction

The endoplasmic reticulum (ER) is a continuum of membrane structures dominating a considerable fraction of the cell volume and forming a pivotal hub for many molecular events such as protein folding, lipid and steroid synthesis, as well as calcium storage[1]. The multifunctional nature of this organelle requires the protection of its integrity under multiple stress conditions to achieve optimal function of individual proteins and the entire organelle[2].

Selective turnover of the ER by autophagy (ERphagy) has emerged as a major quality control pathway ensuring a programmed renovation of the ER through elimination of discrete fragments sequestered in autophagosome and degraded via the lysosomal machinery (macro autophagy)[3]. Receptor-mediated macro autophagy (in the following referred to as autophagy) relies on autophagy receptors selectively recognizing cargo, linking it to the autophagic membrane, and thereby promoting cargo sequestration into autophagosomes. To facilitate this function, most ERphagy receptors are linked to the ER via a transmembrane domain (cargo binding) and in addition harbor a LC3 interaction region (LIR) enabling their binding to members of the LC3/GAPARAP (MAP1LC3 microtubule-associated proteins 1A/1B light chain 3 (LC3) / gamma aminobutyric acid receptor-associated protein) protein family on autophagic membrane[4]. Thus far, eight membrane-embedded ERphagy receptors have been identified: FAM134B/RETREG1[5], SEC62[6], RTN3L[7], CCPG1[8], ATL3[9], TEX264[10], FAM134A/RETREG2 and FAM134C/RETREG3[11], which participate in basal ER turnover, ER re-shaping following stress-related expansion, as well as lysosomal degradation of selected ER proteins[2].

Members of the FAM134 family carry a conserved LIR motif located at their C-terminus and their membrane domain consists of a reticulon homology domain (RHD), comprised of two membrane-embedded hydrophobic regions bridged by a flexible cytoplasmic linker[12]. We recently showed that FAM134 proteins have shared as well as distinct functions and differ in the dynamics of their RHDs[11]. All FAM134 proteins provide critical functions in maintaining

ER homeostasis and their absence results in a massive deformation of the ER network and ER swelling. Although quite alike, the three paralogues may operate differently: while FAM134B constitutively active, FAM134A and FAM134C predominantly exist in an inactive state under basal conditions[11]. Upon ER stress, all three receptors can induce significant ER fragmentation and degradation via the lysosome. However, how FAM134A and FAM134C switch from an inactive to an active state remains elusive. We also demonstrated that FAM134C can act in concert with FAM134B and enhances its activity in degrading misfolded pro-collagen[11]. Likely, the cooperative performance of these two paralogues is tightly regulated through, yet to be explored, processes including post-translational modifications (PTMs) and structural organization. Along these lines, it was recently shown that phosphorylation of the RHD, within the flexible cytoplasmic linker by CAMKII, drives FAM134B oligomerization and promotes ER fragmentation prior to ERphagy[13] however, it is unclear if this phosphorylation event originates from the mTOR (mechanistic target of rapamycin) kinase complex, which is known to be a master regulator of autophagy. It remained also open, how phosphorylation mechanistically drives oligomerization.

Here we show that activity of both FAM134B and FAM134C can be modulated upon inhibition of mTORC1 with Torin1. We analyzed dynamic phosphorylation and ubiquitination of FAM134 proteins upon mTOR inhibition. Several identified phosphorylation sites clustered within the RHD of FAM134 proteins and were positively regulated by Torin1 treatment. In an unbiased kinase screen, we identified CK2 as the downstream kinase for Torin1-induced and FAM134-dependent ERphagy. On the mechanistic level, we show that FAM134B and FAM134C oligomerization is affected upon CK2 inhibition. This suggests phosphorylation-dependent ubiquitination of both proteins as the driving force behind FAM134B and FAM134C clustering.

Results

The ER is a highly dynamic organelle that reacts on environmental changes and stresses with structural remodeling and adaptation of ER-resident protein levels by selective, receptor-mediated macro autophagy of the ER (later referred to as ERphagy).

FAM134C- and FAM134B-driven ERphagy is activated upon mTOR inhibition

Our recent findings showed that FAM134C is an ERphagy receptor working in concert with FAM134B[11]. Since overexpressed FAM134C seemed to be relatively inactive under basal conditions, we hypothesize that mTOR-dependent phosphorylation events activate FAM134B/C-driven ERphagy. To test this hypothesis, we aimed to analyze the impact of mTOR inhibition on FAM134-driven ERphagy flux over time using the ERphagy reporter ssRFP-GFP-KDEL[10] (referred to as KDEL reporter). GFP is rapidly quenched within the acidic environment of lysosomes while RFP fluorescence is preserved. Therefore, changes in RFP/GFP ratio (total integrated fluorescence) can be used to compare ERphagy flux between conditions independent of the monitored cell number (Fig. 1A). Several ERphagy reporters have been identified so far[5–11] and activation of any ERphagy receptor can in principle impact the RFP/GFP ratio. To analyze specifically FAM134-driven ERphagy flux and minimize the impact of other ERphagy receptors, we used U2OS cell lines constitutively expressing the KDEL reporter (CTRL) as well as cells stably overexpressing HA-FLAG-FAM134B (FAM134B) and HA-FLAG-FAM134C (FAM134C) in a doxycycline (DOX)-inducible manner[11]. Under basal conditions (DMSO), overexpression of FAM134B or FAM134C marginally increased ERphagy flux (Fig. 1B). Upon treatment with 250 nM Torin1, ERphagy flux strongly increased over time in all tested cell lines and specifically upon overexpression of FAM134B or FAM134C. Induction of ERphagy flux was approximately 3-folds higher in FAM134B/C overexpressing cells compared to CTRL cells, indicating that the vast majority of measured ERphagy flux results from FAM134B/C-driven ERphagy (Fig. 1B). The

difference between ERphagy flux in FAM134B or FAM134C overexpressing cells and the CTRL cell line represents mTOR-mediated and FAM134-driven ERphagy flux and can serve as a screening window to identify factors important for FAM134B/C activation upon mTOR inhibition.

Kinases involved in mTOR-mediated, FAM134-driven ERphagy

To understand, which downstream kinases regulate mTOR-mediated FAM134B- and FAM134C-driven ERphagy, we screened a library of over 100 probe and probe-like kinase inhibitors as well as available negative controls for their potency to prevent ERphagy induction. These target-optimized inhibitors have a K_i at nanomolar range and the screen was performed uniformly with 1 µM final concentration. After 24h DOX treatment to induce FAM134B and FAM134C overexpression, cells were pre-incubated for 1h with kinase inhibitors to block target kinase activity (-1h) and subsequently treated with 250 nM Torin1 to induce mTOR-mediated ERphagy (0h). Time-point measurements of the ratio of total integrated green (GFP) and red (RFP) fluorescence as well as cell confluence were taken every 2h over a total period of 48h. Heatmaps summarizing the time-resolved screening results on ERphagy flux and cell growth (confluence) are shown respectively in Fig. 1C and Supplementary Fig. 1A. Treatment with several kinase inhibitors prevented Torin1-induced, FAM134B/C-driven, ERphagy. This is indicated by the loss of red color towards higher time points in the heatmap (Fig. 1C). To present screening results in a visually receptive format, data were transformed and normalized: the difference in the RFP/GFP ratio between untreated and Torin1-treated cells was defined as 100% (Supplementary Fig. 1B). Early time points (<12h) were excluded due to the small screening window and subsequent misinterpretation of early data points. The impact of individual compounds was represented as % of relative reduction of FAM134-mediated ERphagy per time point (Supplementary Fig. 1B). Accordingly, HITs were defined as compounds causing >20% relative reduction of ERphagy

over a minimum time period of 12h (6 time points). We identified 10 kinase inhibitors with impact on FAM134B and 15 kinase inhibitors with impact on FAM134C activation, with 8 common HITs (Supplementary Fig. 1C and Supplementary Fig. 3A). From identified HITs, we were specifically interested in those targeting kinases closely related to known mTOR signaling pathway and suppressing both, FAM134B- and FAM134C-mediated ERphagy without inducing obvious cell death. Five candidate compounds corresponded to these criteria: VE-822, KU-6019, CHIR-124 and MK-2206 2HCL and SGC-CK2-1 targeting ATR, ATM, Chk1, Akt, and CK2, respectively (Supplementary Fig. 2A). These kinases were reported to be either related or part of the mTOR signaling axis. For instance, ATM and ATR are members of the phosphatidylinositol 3-kinase PI3-related family (PI3KKs) which also comprises mTOR [14] and CK2 was previously linked to mTOR, as its inhibition was shown to have anticancer effect through downregulation of AKT/mTOR signals [15]. For validation, selected HITs were retested for dose-response. The five selected HIT compounds, VE-822, KU-6019, CHIR-124, MK-2206 2HCL, and SGC-CK2-1 were confirmed and blocked FAM134B as well as FAM134C-mediated ERphagy in a dose-dependent manner (Fig. 2A and Fig. 2B). We also tested the impact of selected HIT compounds on Torin1-induced ERphagy in U2OS CTRL cells. Here, the screening window is relatively narrow. Nevertheless, HIT compounds prevented Torin1-induced ERphagy to certain extent (Supplementary Fig. 2B).

mTOR inhibition triggers phosphorylation of FAM134B and FAM134C by CK2

To identify phosphorylation sites on FAM134B and FAM134C dynamically regulated upon mTOR inhibition, we conducted a SILAC-based mass spectrometry (MS) approach. More specifically, we compared the phosphorylation pattern within individual paralogues under basal and Torin1 treatment (mTOR inhibition). Indeed, several phosphorylation sites were dynamically regulated upon treatment (Fig. 2C), and are highly conserved among species

(Supplementary Fig. 3B). Eight dynamic phosphorylation sites were identified on FAM134C. Four dynamic phosphorylation sites were identified on FAM134B, three clustered within the reticulon homology domain (RHD) and included previously reported functional sites[13]. While this in principle supports the robustness of our MS approach, we were surprised that an inhibitor of the reported Ca2+/Calmodulin-dependent protein kinase II (CAMKII) was absent in the list of our HIT compounds (Fig. 1C and Supplementary Fig. 3A). The previous report tested KN-93, a CaMKII inhibitor with a Ki of 2.58 µM (13). While KN-93 is relatively selective for CaMKII, it has been found to have several off-target effects that potentially impact FAM134-dependent ERphagy flux indirectly, including effects on Ca2+ channels, Ca2+ release, and Calmodulin activity [16]. In our screen another, more potent inhibitor of the kinase CaMKII with a Ki of 0,37 µM was tested (KN-93 phosphate). We reanalyzed both inhibitors in dose-response screens and found doses of >4 µM KN-93 phosphate to impact ERphagy flux over time. KN-93 phosphate showed no effect (defined as >20% relative reduction over min. 12h) till 1 µM (Supplementary Fig. 1D). We analyzed identified phosphorylation sites using a motif-matcher analysis tool (PHOSIDA) [17] to predict kinases and found target sites of casein kinase 2 (CK2) to be the most common (Supplementary Fig. 2C). Specifically, FAM134C may be a target protein for CK2 phosphorylation. This prediction fits to our screening results, where the CK2 inhibitor SGC-CK2-1 was suppressing up to 60% and 70% of Torin1-induced ERphagy in FAM134B and FAM134C overexpressing cells, respectively (Fig. 2A, B).

Phosphorylation by CK2 triggers ubiquitination of FAM134

When immuno-precipitating FAM134C, we noticed three dominant bands >50kDa on a western blot detected with anti-HA antibodies exceeding shifts expected by phosphorylation. Mass spectrometry analysis of corresponding colloidal blue-stained gels (Supplementary Fig. 2D) confirmed the presence of FAM134C peptides in all three gel slices. These findings

indicated posttranslational modifications on FAM134C other than phosphorylation that shift the protein to higher molecular weights. One possibility would be mono- or multi/poly-ubiquitination. To test this hypothesis, we used the TUBE2 system (Fig. 3A), which is able to pull down mono- as well as multi/poly-ubiquitinated proteins. Using lysates of HA-FAM134B and HA-FAM134C overexpressing cells, we were able to identify ubiquitinated FAM134B and FAM134C species, respectively (Fig. 3B). The amount of ubiquitinated FAM134 species increased upon Bafilomycin A1 (BafA1) treatment (Fig. 3B), indicating that ubiquitinated FAM134 proteins indeed undergo ERphagy and therefore accumulate upon blocking autophagy by BafA1 treatment. To test if ubiquitination is functionally important for FAM134-driven ERphagy, we used our ERphagy flux assay and co-treated cells with Torin1 and different concentrations of an E1 inhibitor (MLN7243) blocking the first step of ubiquitin reaction chain. Impairment of the ubiquitin system indeed had a negative impact on ERphagy flux and higher concentration of E1 inhibitor suppressed Torin1-induced ERphagy to more than 80% (Fig. 3C and Fig 3D).

We then asked the question whether activity of CK2 impacts the ubiquitination status of FAM134 proteins. The ubiquitination status of FAM134B and FAM134C upon Torin1 treatment was analyzed in the presence and absence of CK2 inhibitor and compared it to basal conditions (DMSO). Along the hypothesis that ubiquitination of FAM134 is promoting ERphagy, a higher amount of ubiquitinated FAM134B and FAM134C were found upon Torin1-mediated ERphagy induction (Fig. 3E). However, the difference between basal and induced conditions was much more pronounced for FAM134B than for FAM134C. High molecular species disappeared upon co-treatment of Torin1 and CK2 or treatment with E1 inhibitor, indicating that phosphorylation is a prerequisite for ubiquitination of FAM134 proteins.

Receptor oligomerization is thought to be important to drive vesiculation/fragmentation of the ER and subsequently delivery to the lysosome[18]. We hence investigated the ubiquitination

status of oligomerized FAM134 proteins by performing immuno-precipitation experiments using the Venus system (Supplementary Fig. 3C). Two constructs were generated, carrying FAM134B or FAM134C fused to one half of a GFP molecule. After transient co-transfection of both constructs, FAM134 proteins oligomerize and split GFP molecules can fuse to form a complete and stable GFP molecule. We immunoprecipitated FAM134B or FAM134C homo-dimers using GPF-trap beads and detected for ubiquitin. Again, we were able to detect high-molecular weight species of FAM134B and FAM134C under basal and induced conditions (Fig. 3F). These may represent SDS-resistant dimers as suggested previously [13], as well as highly multi/poly-ubiquitinated FAM134 proteins. The detected ubiquitination signal completely vanished upon inhibition of CK2, further supporting our hypothesis that CK2-dependent phosphorylation events are a prerequisite for ubiquitination of FAM134B and FAM134C.

Phosphorylation increases FAM134 nanoscale cluster size

We investigated the impact of RHD phosphorylation on nanoscale clustering (nanoscale distribution: 50-200 nm) of FAM134 proteins using single-molecule localization microscopy (SMLM), an optical super-resolution method that achieves near-molecular resolution and enables quantitative read-out[19]. For this purpose, we used optimized sample preparation conditions with 12h induction of mild HA-FAM134 overexpression by doxycycline, followed by 6h treatment with DMSO, Torin1, and Torin1+CK2 inhibitor, respectively. Using DNA point accumulation in nanoscale topography (DNA-PAINT 2), we imaged FAM134 clusters smaller than the resolution limit of light microscopy (Fig. 4A, B). A quantitative analysis of FAM134B nanoscale clustering using the DBSCAN clustering algorithm 3 revealed a unimodal distribution of cluster diameters under basal conditions (mode = 66 nm, σ = 0.23) (Fig 4C). Upon Torin1 treatment, a second cluster population emerged at a larger cluster diameter (mode = 104 nm, σ = 0.24). Cotreatment with CK2 inhibitor prevented the formation

of the larger nanoscale cluster population, while retaining the first population of small clusters (mode = 69 nm, σ = 0.23), indicating that FAM134B cluster size is mediated and regulated by CK2 activity. A quantitative analysis of FAM134C nanoscale cluster diameters also showed a unimodal, yet broader distribution under basal conditions (mode = 52 nm, σ = 0.52). In contrast to FAM134B, Torin1 treatment did not lead to the emergence of a second population of FAM134C clusters with larger diameter (mode = 53 nm, σ = 0.51) (Fig. 4D). At the same time, statistical analysis revealed a small, significant change of the cluster diameter, which was reversed by co-treatment with CK2 inhibitor (Fig. 4D, Supplementary Fig. 4A).

The impact of CK2 inhibitor on FAM134 cluster diameters can be caused by direct (phosphorylation of FAM134) or indirect actions (phosphorylation of other proteins within the same signaling cascade, up-/down-regulation of proteins involved, etc.). In order to support a direct regulation of FAM134 by CK2, we mutated some of the serine sites within the RHD domain of FAM134B and FAM134C, which were shown to be dynamically phosphorylated upon Torin1 treatment. Single-molecule imaging and cluster analysis was repeated with the respective alanine mutants (phospho-mutants). FAM134B phospho-mutant cluster diameters showed a similar distribution as FAM134B WT under basal conditions (mode = 63 nm, σ = 0.17). However, in contrast to their WT counterpart, FAM134B phospho-mutant cluster size did not change upon Torin1 treatment (mode = 65 nm, σ = 0.19) (Fig. 4C). This indicates that the mutated phosphorylation sites have a direct impact on FAM134B function and that CK2-mediated phosphorylation drives/boosts the formation of larger FAM134B nanoscale clusters upon ERphagy induction by Torin1. As for the wildtype form of FAM134C, we did not observe a strong impact of CK2 inhibition on FAM134C S258A cluster diameters (Fig. 4D), indicating that phosphorylation of serine 258 has regulatory functions that are not directly related to FAM134C cluster size.

CK2 mediated phosphorylation regulates FAM134 protein density within nanoscale clusters

The amount of FAM134 proteins within nanoscale clusters may vary between clusters of the same size, dependent on the space between individual FAM134 proteins (Fig. 4A, Fig. 5). Close packing of FAM134 proteins (high density) may be required for their ERphagy function, e.g. bending of the ER membrane to facilitate efficient fragmentation[12] To further refine the characteristics of nanoscale clusters, we analyzed the relative protein density within FAM134 nanoclusters by extracting the number of single-molecule binding events (localizations) for different conditions and phosphorylation states (phospho-mutants) (Fig. 4E-J). The rationale behind this analysis is that an increase in protein density leads to a corresponding increase of single-molecule localizations detected per nanoscale cluster. As expected, we detected increasing numbers of localizations for all conditions (Fig. 4E-J). A direct comparison of wildtype and FAM134 phospho-mutants showed that clusters with high numbers of localizations were largely absent for the inactive phospho-mutants (colored dots versus black triangles). We then identified high-density FAM134 wildtype clusters by thresholding (>100 localizations/cluster, cluster diameter > 90 nm; grey regions). For FAM134 B, the amount of high-density clusters (as percentage of all analyzed clusters) increased upon Torin1 treatment (5.6 %) compared to basal conditions (2 %) and CK2 inhibition (3.7 %) (Fig. 4E-G and Supplementary Fig. 4B-D). Interestingly, we measured only a minor increase of high-density clusters for FAM134C after Torin1 treatment (6.6 % for DMSO and 7.3%) but a strong decline after CK2 inhibition (2.6 %) (Fig. 4H-J and Supplementary Fig. 4E-G). This indicates that FAM134C is already regulated by CK2 under basal conditions. Subdividing nanoscale clusters in small (30-90 nm), medium (90-150 nm) and large clusters (> 150 nm) and plotting the relative frequency distribution of localizations per cluster refined the distribution of high-density (Supplementary Fig. 4B-G).

Together, these findings reflect higher FAM134B densities upon Torin1-induced phosphorylation and hint to a dynamic process, where FAM134B clusters reach a certain size (>90 nm) and then get further activated (by phospho-dependent ubiquitination) to increase the density of included molecules. In line with this hypothesis, nanoscale clusters formed by phospho-mutants of FAM134B and FAM134C were able to reach a size of >150 nm, but were unable to further mature to respective high-density clusters (Fig. 4E-J). Combining this with our findings that CK2 inhibition upon Torin1 treatment suppresses ERphagy flux (Fig. 2A, B), we predict that only high-density clusters are functionally active in respect of ER fragmentation and subsequent delivery to the lysosome (Fig. 5).

Discussion

One of the challenging questions in the ERphagy field is how the pathway is fine-tuned, starting from the initial trigger to initiate ER curvature towards ER fragmentation and final delivery to the lysosome. It is obvious that ERphagy receptors play a critical role along this path, but the molecular mechanisms that drive their activation and functions remain poorly understood. In this manuscript, we provide evidence that phosphorylation-mediated ubiquitination of FAM134B and FAM134C is essential for the formation of high-density clusters of FAM134 proteins on the ER membrane and subsequent FAM134-driven ERphagy. These findings originated from our previous reports that FAM134C is held in an inactive state under basal conditions and may serve as an enhancer of FAM134B-dependent ERphagy flux upon stress [11]. We hypothesized that an mTOR-mediated phosphorylation cascade can serve as an activation signal for FAM134-driven ERphagy. An unbiased screen against a chemical library of kinase inhibitors modulating ERphagy flux revealed ATR, ATM, Chk1, Akt, and CK2 to be downstream of and essential for mTOR-mediated induction of FAM134B- and FAM134C-driven ERphagy. In addition, we identified dynamically regulated phosphorylation sites upon Torin1 treatment within the RHD domain and adjacent regions of FAM134B and

FAM134C. In line with our chemical screen, target site prediction suggests CK2 to be the kinase phosphorylating FAM134 proteins. CK2 is known to be ubiquitously expressed and a constitutively active kinase that regulates a number of biological processes [20]. In addition, CK2 has been linked to autophagy-related diseases such as Alzheimer, Parkinson, and Huntington disease. In this study we attributed to CK2 a function in orchestrating FAM134B- and FAM134C-induced ERphagy by mediating phosphorylation of specific sites that drive clustering of ERphagy receptors and promoting ERphagy flux. Phosphorylation of FAM134B and subsequent induction of its oligomerization was previously reported and at that time linked to CaMKII activity[13]. Within our settings, CaMKII inhibition performed poorly in terms of preventing FAM134B-driven ERphagy, while CK2 inhibition had a strong effect. However, our findings do not rule out a possible cooperation between CK2 and CaMKII kinases in fine-tuning these events, specifically since CAMKII was previously shown to form a complex with CK2[21]. Mechanistically, phosphorylation could alter the structure and create new binding interfaces both in membrane as well as on cytosolic domains of FAM134 proteins.

At the same time, we showed that FAM134B and FAM134C are ubiquitinated in an mTOR- and CK2-dependent manner. Phosphorylation may therefore create a new cytosolic binding surface important for the recruitment and/or activation of ligases. Accumulation of ubiquitinated FAM134 proteins upon autophagy inhibition (Bafilomycin1 treatment) indicate that ubiquitination of FAM134 proteins is not related to ER associated protein degradation of overexpressed FAM134 via the proteasome, but has functional relevance for FAM134-driven ERphagy. We therefore hypothesize that ubiquitination is needed for the regulation and/or activation of FAM134-driven ERphagy. In agreement with this hypothesis, inhibition of the ubiquitination system (treatment with E1 inhibitor) suppressed mTOR-mediated, FAM134-driven ERphagy flux. Treatment with CK2 inhibitor abolished ubiquitination of FAM134B

and FAM134C, indicating that ubiquitination is downstream to CK2-dependent phosphorylation and that phosphorylation by CK2 is a prerequisite of FAM134 ubiquitination. Previous studies suggested that super clustering of RHD-containing receptors e.g. Atg40 in the yeast and FAM134B in mammals generates high-curved regions that subsequently can pinch-off the ER and get delivered to the lysosome[12,22]. Our data implies an interesting chain of reactions where phosphorylation and subsequent ubiquitination may be involved in the regulation and formation of such super receptor clusters. To dissect the consequences of posttranslational modifications on oligomerization, we analyzed two parameters of nanoscale clusters (50-200nm) of either wild type or phospho-mutants of FAM134 proteins by super resolution microscopy: changes in cluster diameter (size) and differences in localizations within a cluster of a specific size (density of FAM134 molecules). Nanoscale clusters of FAM134 wt proteins changed from a unimodal (DMSO/basal) to a bimodal distribution upon induction of ERphagy (Torin1). The emerging population upon induction clustered around 104 nm ($\sigma = 0.24$), indicating that a cluster size of > 90nm is necessary for mTOR-mediated, FAM134B-driven ERphagy. Since the appearance of the larger FAM134B cluster population was suppressed by CK2 inhibition as well as mutation of phospho-sites, phosphorylation and/or subsequent ubiquitination is essential for its formation. In contrast, the size distribution of clusters built by FAM134C wt or phospho-mutant was similar in all tested conditions.

We also found that the density of FAM134 molecules in clusters >90 nm started to vary, both in FAM134B- as well as FAM134C-formed clusters. This finding hints to a mechanism, where clusters first grow to a certain size and then further mature by increasing the density of FAM134 molecules within the cluster. The increase in local concentration of FAM134 proteins may be needed to sufficiently bend the ER membrane to initiate vesiculation. Along this line, maturation to high-density FAM134B clusters increased approximately 3-fold upon ERphagy induction (2% vs. 5.6% relative abundance) and was largely suppressed by treatment with CK2 inhibitor (3.7%). Interestingly, FAM134C was already forming high-

density clusters under basal conditions (6.6%) and their relative abundance only slightly increased upon ERphagy induction (7.3%). At the same time, co-treatment with CK2 inhibitor did reduce their abundance considerably to levels below basal conditions (2.6%), indicating that also FAM134C oligomerization is regulated by CK2-dependent phosphorylation. These findings are in alignment with the ubiquitination status of both FAM134B as well as FAM134C: the ubiquitination level of FAM134B is little under basal conditions and strongly increases upon Torin1 treatment, while FAM134C is already ubiquitinated under basal conditions and its ubiquitination level only slightly increases upon mTOR inhibition.

Together our data shows that mTOR-mediated phosphorylation by CK2 as well as phospho-dependent ubiquitination of FAM134 proteins play essential roles in the regulation and activation of FAM134B- and FAM134C-driven ERphagy. In this context we suggest that only high-density nanoscale clusters >90nm are functionally active during ERphagy. For future studies we hypothesize that phospho-dependent ubiquitination facilitates the formation of high-density FAM134 clusters, presumably by introducing conformational changes between adjacent FAM134 molecules and/or by recruiting cytosolic factors with oligomerizing properties to the forming ER vesicle. As FAM134C serves as an enhancer of FAM134B (REF), we further hypothesize that pre-existing, ubiquitinated FAM134C nanoscale clusters may serve as collection points for substrates and subsequently as nucleation points for FAM134B and that this is the reason behind the rapid occurrence of a second, larger FAM134B cluster population upon Torin1 treatment.

Material and methods

Reagents and antibodies:

Kinase inhibitor library was provided by the SGC Frankfurt donated probes program and complemented by additional kinase inhibitors. Torin1 was purchased from_Bio-techne, 4247 and Bafilomycin A1 from Cayman Chemical Corporation, 11038. Following primary

antibodies were used for immunoblotting and immunofluorescent staining: rabbit anti-HA tag (Cell signalling, C29F4), rat anti-HA tag (Roche, 11867432001), rabbit anti-CK2 (ThermoFicsher Scientific, PA5-27426), mouse anti-ubiquitin PD4 (abcam, ab7254), mouse anti-LC3B (MBL, PM036), rabbit anti-GAPDH (Cell signalling 2118L). Following secondary antibodies were used for immunoblotting: anti-mouse (Thermo Fisher Scientific, 31326) anti-rabbit (Thermo Fisher Scientific, 32460) anti-rat (Cell signalling, 70775). Following secondary antibodies were used for immunofluorescent staining for super-resolution microscopy: anti-rabbit (AffiniPure, 711-005-152) and anti-mouse (AffiniPure, 115-005-003), covalently labeled with short oligonucleotide strands anti-P1 (5´-ATCTACATATT-3´) and anti-P5 (5´-TATGTAACTTT-3´), respectively.

Plasmid

pCW57-CMV-ssRFP-GFP-KDEL was a gift from Noboru Mizushima (University of Tokyo, Tokyo, Japan), (Addgene plasmid # 128257 ; RRID: Addgene_128257). pLenti CMV GFP Hygro (656-4) was a gift from Eric Campeau and Paul Kaufman (Addgene plasmid # 17446; http://n2t.net/addgene:17446; RRID:Addgene_17446). pLenti CMV GFP Hygro (656-4) was used as the backbone to create pLenti-CMV-Hygro- ssRFP-GFP-KDEL for consecutively expressing ssRFP-GFP-KDEL. Briefly, pLenti CMV GFP Hygro (656-4) was digested with two restriction enzymes (BamHI and SalI) to remove the GFP cassette. ssRFP-GFP-KDEL was then amplified by PCR and cloned into pLenti CMV GFP Hygro (656-4) plasmids using Sequence and Ligation Independent Cloning (SLIC) with T4 DNA polymerase. iTAP-FLAG-HA-FAM134B (also referred to as pMCSV-puro-FLAG-HA-FAM134B) and iTAP-FLAG-HA-FAM134B (also referred to as pMCSV-puro-FLAG-HA-FAM134C) were gifts from Ivan Dikic (Goethe University Frankfurt am Main, Germany). iTAP-FLAG-HA-FAM134B and iTAP-FLAG-HA-FAM134C were used as the backbone to create different phosphorylation mutants using quick-change PCR mutagenesis.

Cell culture

U2OS Trex and HEK293T cells were maintained in a 37°C incubator with humidified 5% CO2 atmosphere and cultured in Dulbecco's modified Eagle's medium (DMEM) (Thermo Fisher Scientific) supplemented with 10% fetal bovine serum (FBS) (Thermo Fisher Scientific) and 100 U/ml penicillin and streptomycin (PS) (Thermo Fisher Scientific). U2OS Trex cells stably expressing ssRFP-GFP-KDEL and inducibly individual FAM134 proteins were described previously [11]. These cells were treated with 1 µg/ml of doxycycline (Sigma-Aldrich, D9891) to induce FAM134 protein expression. Prior to each treatment, cells were plated the day before in order to perform the experiments when cells had a final confluency of 70-80%. HEK293T was purchased from ATCC and were used for transient transfections. For transient expression, DNA plasmids were transfected with JetPEI (Polyplus, 101000020) according to manufacturer instructions.

Cell line generation

U2OS Trex cells were a gift from Stephen Blacklow (Brigham and Women's Hospital and Harvard Medical School) [23] and were culture using DMEM supplemented with 10% FBS, 1% PS and 15 µg/ml Blascitidin (Thermo Fisher scientific, A1113902). Lentiviral particles were produced in HEK293T cells using pLenti-CMV-Hygro-ssRFP-GFP-KDEL and pMD2.G and psPAX2. Retroviral particles were produced in HEK293T using iTAP-FLAG-HA plasmids expressing FAM134B, FAM134C or different phosphorylation mutants, packaging plasmid (pCMV-Gag-Pol) and the envelope plasmid (pCMV-VSV-G). The U2OS Trex cells were plated and propagated in 6 well-plates overnight. On the next day, transduction with viruses was performed. Two days later, transduced cells with iTAP-FLAG-HA plasmids were selected using 15 µg/ml Blaticidin and 2 µg/mL puromycin (Invitrogene, Thermo Fisher Scientific, Waltham, Massachusetts, USA) for 3 passages. U2OS Trex cells expressing

FAM134B, FAM134C or different mutants were used for transduction with ssRFP-GFP-KDEL retroviruses. The transduced cells were selected using 15 µg/ml Blasticidin, 2 µg/mL puromycin and 150 µg/ml Hygromycin B. Afterward, the cells were sorted for different populations of RFP- and GFP-expressing cells using SH800S Cell Sorter (Sony Biotechnology, San Jose, CA, USA). Stable clones were maintained in the same medium as used for selection.

Co-immunoprecipitation

U2OS cells stably expressing FAM134 proteins were induced with doxycycline (1 µg/ml) for 24 h. Following treatments (DMSO (Sigma-Aldrich), Torin1 (Bio-techne), CK2 inhibitor (SGC donated probes), Bafilomycin A1 (Cayman Chemical Corporation)), confluent 10 cm diameter petri dishes of U2OS cells were harvested in 500 µL of ice-cold lysis buffer: 50 mM Tris/HCl (pH 8.0), 120 mM NaCl, 1 % (v/v) NP40 (Merck Millipore), cOmplete protease inhibitor cocktail (Roche), phosphatase inhibitor cocktail 1 & 2 (Sigma-Aldrich). Lysates were cleared by centrifugation at 20000 x g for 15 min at 4°C and 1 mg of proteins was incubated overnight at 4°C with monoclonal anti-HA-agarose antibody (Thermo Scientific) with constant mixing. Beads were then washed 3 times in wash buffer [0.1% (v/v) NP40], resuspended in SDS sample buffer and boiled at 95°C for 10 min. Beads were collected by centrifugation at 2500 × g for 2 min and supernatants were loaded on SDS-PAGE and western blot was performed using the indicated antibodies.

GFP trap pulldown

HEK293T cells were transiently cotransfected with two constructs carrying either FAM134B or FAM134C each independently tagged with half GFP at the N-terminus. Following 6h treatment with the indicated conditions, cells were washed with 1x PBS and lysed in ice-cold lysis buffer containing 50 mM Tris pH 7.5, 150 mM NaCl, 5 mM EDTA pH 8.0, 1% Triton

X-100 supplemented with cOmplete protease inhibitor cocktail, phosphatase inhibitor cocktail 1 & 2 and deubiquitinase inhibitor (NEM). Samples were incubated on ice for 15 min and centrifuged at 20000 × g for 15 min at 4 °C. GFP Trap beads were equilibrated and washed 3 times in 500µL of ice-cold lysis buffer and were spun down at 2500 × g for 2 min at 4 °C. In total, 1 mg of lysates was added to 5 µl of equilibrated GFP Trap beads and incubated overnight 4 °C with constant mixing. Tubes were spun at 2500 × g for 3 min at 4 °C. GFP Trap beads were washed three times with 500 µl ice-cold lysis buffer. 50 µL of 2× SDS sample buffer was then added to the GFP Trap beads and were boiled for 10 min at 95 °C. Beads were collected by centrifugation at 2500 × g for 2 min and SDS-PAGE was performed with the supernatant.

Tandem Ubiquitin Binding Entities 2 (TUBE2) assay

FAM134 proteins expression was induced with 24h doxycyclin (1 µg/ml) treatment. Following treatments (DMSO, Torin1, CK2 inhibitor, Bafilomycin A1), confluent 10 cm diameter petri dishes of U2OS cells were harvested in 500µL of ice-cold lysis buffer: 50 mM Tris/HCl (pH 8.0), 120 mM NaCl, 1% (v/v) NP40, cOmplete protease inhibitor cocktail, phosphatase inhibitor cocktail 1 & 2. Lysates were cleared by centrifugation at 20000 x g for 15 min at 4°C and 1mg of proteins was incubated overnight at 4°C with 10 µL of agarose-TUBE2 resin. Reactions were rotated overnight at 4°C, washed three times with NP40 buffer and analysed by SDS-PAGE. HA antibody was used to detect FAM134 proteins and ubiquitinated species.

Immunoblotting of total cell lysates

Cells were harvested after removing the culture medium and washing with 1X PBS and lysed in lysis buffer (150 mM NaCl, 50 mM Tris-HCl pH 7.5, 10 mM NaF, 1 mM EGTA, 5 mM $MgCl_2$, 0.1% SDS) supplemented with protease and phosphatase inhibitors. Insoluble cell

components were separated at 20000 × g for 15 min at 4°C and total protein concentration was assessed using BCA assay (Thermo scientific). Protein denaturation was performed in SDS sample buffer at 95 °C for 10 min.

Protein lysates were resolved in SDS-PAGE gels and transferred to PVDF (Millipore, 0.2µm) membrane. Membranes were saturated in PBST 0.1% Tween containing 5% BSA and incubated overnight at 4°C with the specific primary antibody.

Phospho-Mass spectrometry and SILAC labeling

U2OS cells stably expressing FAM134 proteins were cultures for 3 weeks in SILAC media supplemented with 10% fetal bovine serum, 100 U/ml penicillin and streptomycin and labelled amino acids (L-arginine (Arg0), L-lysine (Lys0), L-arginine- U-^{13}C6 99% (Arg6), L-lysine-4,4,5,5-D4 96–98% (Lys4), L-arginine-U-^{13}C6-^{15}N4 99% (Arg10), L-lysine- U-^{13}C6-^{15}N2 99% (Lys8)). To induce FAM134 protein expression, labelled U2OS cells were treated with doxycycline for 24h. Light-, Medium- or heavy-labeled cells were subjected to indicated conditions and harvested in ice-cold lysis buffer: 50 mM Tris/HCl (pH 8.0), 120 mM NaCl, 1% (v/v) NP40, cOmplete protease inhibitor cocktail, phosphatase inhibitor cocktail 1 & 2. Lysates from individual labelled cell lines were cleared by centrifugation at 20000 x g for 15 min at 4°C and mixed 1:1:1 ratio (light/medium/heavy) prior to overnight incubation at 4°C with monoclonal anti-HA-agarose antibody with constant mixing. Beads were then washed 3 times and bait proteins (FAM134s) were either directly trypsin digested on-beads or in gel and peptides were analysed by LC-MS/MS. The mass spectrometry proteomics data have been deposited to the ProteomeXchange Consortium via the PRIDE [30] partner repository with the dataset identifier PXD036103.

Username: reviewer_pxd036103@ebi.ac.uk
Password: xzKnvXdk

ERphagy flux assay

U2OS TRex FLAG-HA-FAM134s stable and inducible cell lines were infected with lentivirus carrying the pCW57-CMV-ssRFP-GFP-KDEL (Addgene #128257). We previously deleted the tetracycline response element, via PCR, from ssRFP-GFP-KDEL in order to have constitutive expression. Wild-type and *Fam134*s knockout MEFs were infected with pCW57-CMV-ssRFP-GFP-KDEL (Addgene #128257) in order to generate ERphagy reporter inducible cell lines. Fluorescence of GFP and RFP as well as cell confluence (phase) was monitored over time via the IncuCyte S3 (Sartorius, Germany) in 384-well format. 1500 cells (U2OS) per well were seeded in 50µl DMEM media, supplemented with 10% Fetal Bovine Serum (FBS) 1% Penicillin/Streptomycin, 2 µg/ml Puromycin, 15 µg/ml Blasticidin 1 µg/ml doxycycline and incubated for 24h before treatment. For indicated treatments, 50 µl of media containing indicated treatments were added. Between the actual treatment and the first scan point (0hrs) appx. 5-10min passed for technical reasons. Screens in all three channels were taken at indicated time points following the treatment. ERphagy flux was monitored through changes in the ratio of the total fluorescence intensity of RFP/GFP. Each point represents the averaged ratio of data obtained from three individual wells (technical replicates). Metadata from all screening experiments can be found under: https://hessenbox-a10.rz.uni-frankfurt.de/getlink/fiGhFF11N4Mj2Csm47H4P3ip/Screening_data.zip.

Antibody-oligonucleotide conjugation for DNA-PAINT

Secondary antibodies donkey anti-rabbit (AffiniPure, 711-005-152) and goat anti-mouse (AffiniPure, 115-005-003) were covalently labeled with short oligonucleotide strands anti-P1 (5´-ATCTACATATT-3´) and anti-P5 (5´-TATGTAACTTT-3´), respectively, via DBCO-

sulfo-NHS ester chemistry. In brief, concentrated secondary antibodies were incubated with a 20-fold molar excess of DBCO-sulfo-NHS ester (Jena Bioscience, CLK-A124-10) for 90 min at 4°C. Excess reagent was removed using spin filters (Merck, Germany) and docking strand labeled antibodies were incubated with a tenfold molar excess of azide-functionalized DNA-docking strands overnight at 4°C. Samples were then filtered through Amicon centrifugal filters (100.000 MWCO) to remove unbound oligonucleotides and change storage buffer to PBS. Finally, antibody-DNA complexes were concentrated to 5 mg/mL and stored at 4°C.

Sample preparation for exchange DNA-PAINT

For exchange DNA-PAINT experiments, U2OS cells were seeded in fibronectin coated Ibidi µ-slide VI chambers at a density/confluence of 60% and FAM134s protein expression was induced with 1µg/ml Dox overnight. Cells were chemically fixed with prewarmed (37°C) 4% methanol-free formaldehyde (Sigma-Aldrich, Germany) in PBS for 20 min followed by three washing steps with PBS. Primary antibodies rabbit anti-HA (1:500) and mouse anti-LC3B (1:200) were subsequently added in permeabilization/blocking buffer (10% FCS (Gibco), 0.1% saponin (Sigma)) and incubated for 60 min at room temperature. Excess primary antibodies were removed from the chambers by three washing steps with PBS and custom docking-strand labeled secondary antibodies (1:100 in permeabilization /blocking buffer) were added to the chambers. After incubation for 60 min at room temperature, samples were washed thrice to remove excess secondary antibodies. Finally, samples were post-fixed using 4% methanol-free formaldehyde in PBS for 10 min at room-temperature followed by three washing steps with PBS. For colocalization experiments, fiducial markers were used for image registration (125 nm gold beads (Nanopartz, USA). Gold beads were sonicated for 10 min and diluted 1:30 in PBS. Diluted samples were again sonicated for 10 min and 100 µL of the solutions were added to the microscopy chambers. After settlement of the gold beads (5 min), the samples were washed thrice with PBS. Cell chambers were finally assembled to a

microfluidic device (Bruker, USA) for automated buffer exchange. Prior to image acquisition, ATTO-655 labeled imager Strands P1 or P5 (400 pM, 0.5 M NaCl, PBS, pH 8.3) were injected to the flow chamber at a flow rate of 600 µl/min. For colocalization experiments imager strands were exchanged by washing the samples with 1 mL PBS followed by injection of new imager strands.

Microscopy setup and data acquisition

DNA-PAINT based super-resolution microscopy was performed at the N-STORM super-resolution microscopy system (Nikon, Japan), equipped with an oil immersion objective (Apo, 100x, NA 1.49) and an EMCCD camera (DU-897U-CS0-#BV, Andor Technology, Ireland) as described previously[24]. Fluorophore-conjugated oligonucleotides were excited with a collimated 647 nm laser beam at an intensity of 2 kW/cm^2 (measured at the objective) at highly inclined and laminated optical sheet (HILO) mode. 40.000 and 20.000 consecutive frames were acquired for imager strands P1 (5´-TAGATGTAT-3´-ATTO655) and P5 (5´-CATACATTGA-3´-ATTO655), respectively. Image acquisition was performed at 20 Hz (P1) and 10 Hz (P5) in active frame transfer mode with an EMCCD gain of 200, a pre amp gain of 1 and at an effective pixel size of 158 nm. A customized cylindrical lens (RCX-39.0.38.0-5000.0-C-425-675, 10 m focal length, CVI Laser Optics, UK) was inserted into the emission light path of the optical setup for astigmatism-based 3D exchange DNA-PAINT experiments. Software tools NIS Elements (Nikon, Japan), LCControl (Agilent, USA), and Micro-Manager 1.4.22 [25] were used for control of the optical setup and image acquisition. FAM134B and FAM134C were imaged sequentially using a microfluidic assisted exchange of imager strands. The spatial resolution of our super-resolution images was determined to 22 ± 2 nm (mean ± s.d.,[26], allowing the detection of FAM134 nanoscale cluster.

Image processing

Localization of single molecules and reconstruction of super-resolution images were performed with modular software package Picasso[27]. Integrated Gaussian maximum likelihood estimation was used for detection of single molecules using the following parameter: Min. net. gradient of 15000, a baseline of 205, a sensitivity of 4.78, a quantum efficiency of 0.95. Sample drift correction and image alignment were performed via redundant cross-correlation algorithm using fiducial marker. For FAM134B (wt and S149-151-153A) and FAM134C S258A, localizations were subsequently filtered based on ATTO-655 single-molecule footprint (PSF symmetry 0.6 < FWHM(x)/FWHM(y) < 1.4). Signals from the same origin detected in consecutive images were linked within a radius of five times the nearest-neighbor based analysis (NeNa)[28] localization precision and a maximum dark time of 8 consecutive frames. Remaining signals from fiducial marker were removed by excluding traces from the same origin with a length larger than 20 consecutive frames and a min. net gradient < 100.000. To account for the high expression level in FAM134C wt expressing cells, nanoscale cluster were first segmented from ER-located background signal via Density-based spatial clustering and application with noise algorithm[29] analysis using a radius of 16 nm and a minimum density of 30 localizations followed by data filtering as described previously.

For exchange 3D DNA-PAINT experiments a 3D calibration curve was recorded at the microscope using z-stacks (z-stack step size 50 nm) of surface-immobilized TetraSpeck Microspheres (0.1 µm, Thermo Fisher Scientific) and analyzed in Picasso software. The axial section was limited to 800 nm. FAM134C and LC3B-II 3D were aligned after sequential imaging in Picasso software using fiducial marker and finally visualized in ViSP open source software.

Cluster analysis

DBSCAN algorithm was used to identify protein nanocluster in DNA-PAINT super-resolution images. A radius of 32 nm (FAM134B wt and S149-151-153A and FAM134C

S258A) and 64 nm (LC3B-II) and a minimum density of 10 localizations were used as parameter. For FAM134C wt, a radius of 16 nm and a minimum density of 5 localizations were used for DBSCAN analysis. For the determination of nanoscale cluster density in U2OS cells, protein clusters were normalized with respect to the cell area. Therefore, cell contours were drawn in super-resolution images using ImageJ and the cell area was determined. For colocalization analysis of FAM134B/C and the autophagosomal membrane marker LC3B-II we used custom-writer analysis tools in Python 3.7 (analysis program available under https://github.com/MariusGlg/ClusterColocAnalyzer.git). In brief, we calculated the Euclidean distance between all FAM134B/C and LC3B-II cluster centroids in a super-resolution image. Based on a threshold (158 nm) FAM134B/C and LC3B-II colocalization pairs were identified. If multiple LC3B-II were allocated to a single FAM134B/C cluster, cluster pairs with the shortest Euclidean distance were chosen for further analysis. FAM134B/C located in such cluster were further characterized with respect to cluster diameter.

Statistical analysis

FAM134B and FAM134C nanocluster diameter were tested for normal distribution via Shapiro-Wilk normality test and statistical significance via non-parametric Mann-Whitney U-test. The relative frequency distribution of nanocluster diameter was fitted with a Log-normal distribution and the mode of distribution was calculated as $e^{(\mu-\sigma^2)}$. All statistical analysis were performed in OriginPro (Origin Lab).

Acknowledgements

We thank the mass spectrometry unit of IBC2, in particular Georg Tasher, Rajeshwari Rathore, and Martin Adrian-Allgood for great technical support. We thank Ivan Dikic for critical comments on the text as well as Stefan Knapp and Andreas Krämer for providing tools

and reagents as well as To Dinh Nguyen Ngu for technical support in compound handling. This work was supported by the German Research Foundation DFG (SFB1177/2 (RB, HHX, MG, PSM, TJ, PB, VD, MH, AS), HE 6166/17-1 (MG, MH), and WO210/20-2 (AS)) the AIRC (MFAG 24856) and Telethon Foundation (PG), the Dr. Rolf M. Schwiete Stiftung (13/2017) (AS), the Hessian Ministry of Science and Art (HMWK) initiative ENABLE, the Bundesministerium für Bildung und Forschung (BMBF) initiative PROXIDRUGS (03ZU1109HA), and the EU/EFPIA/OICR/McGill/KTH/Diamond Innovative Medicines Initiative 2 Joint Undertaking (EUbOPEN grant n° 875510) (AS).

Data availability

Mass spectrometry data is available via PRIDE (PXD036103; Username: reviewer_pxd036103@ebi.ac.uk; Password: xzKnvXdk). All screening meta data obtained with the Incucyte® can be found under https://hessenbox-a10.rz.uni-frankfurt.de/getlink/fiGhFF11N4Mj2Csm47H4P3ip/Screening_data.zip. Raw images of super-resolution microscopy can be made available upon request.

Discloser statement

The authors declare no conflict of interest.

Authors contribution

RB: conceptualization, investigation, formal analysis, visualization, writing – original draft preparation; HHX: investigation, validation, writing – review & editing MG: methodology, investigation, formal analysis, visualization, writing – review & editing PSM: investigation, formal analysis, data curation SC: investigation, validation TJ: investigation, formal analysis AG: resources TG: investigation PB: supervision VD: methodology PG: validation, resources, writing – review & editing; MH: methodology, supervision, writing – review & editing,

funding acquisition AS: conceptualization, methodology, validation, data curation, visualization, writing – original draft preparation, supervision, project administration, funding acquisition

References

1. Schwarz, D. S. & Blower, M. D. The endoplasmic reticulum: Structure, function and response to cellular signaling. *Cellular and Molecular Life Sciences* vol. 73 79–94 Preprint at https://doi.org/10.1007/s00018-015-2052-6 (2016).
2. Chino, H. & Mizushima, N. ER-Phagy: Quality Control and Turnover of Endoplasmic Reticulum. *Trends in Cell Biology* vol. 30 384–398 Preprint at https://doi.org/10.1016/j.tcb.2020.02.001 (2020).
3. Stolz, A. & Grumati, P. The various shades of ER-phagy. *FEBS Journal* vol. 286 4642–4649 Preprint at https://doi.org/10.1111/febs.15031 (2019).
4. Hübner, C. A. & Dikic, I. ER-phagy and human diseases. *Cell Death and Differentiation* vol. 27 833–842 Preprint at https://doi.org/10.1038/s41418-019-0444-0 (2020).
5. Khaminets, A. *et al.* Regulation of endoplasmic reticulum turnover by selective autophagy. *Nature* **522**, 354–358 (2015).
6. Fumagalli, F. *et al.* Translocon component Sec62 acts in endoplasmic reticulum turnover during stress recovery. *Nature Cell Biology* **18**, 1173–1184 (2016).
7. Zhang, H. *et al.* Full length RTN3 regulates turnover of tubular endoplasmic reticulum via selective autophagy. doi:10.7554/eLife.25555.001.
8. Smith, M. D. *et al.* CCPG1 Is a Non-canonical Autophagy Cargo Receptor Essential for ER-Phagy and Pancreatic ER Proteostasis. *Developmental Cell* **44**, 217-232.e11 (2018).

9. Chen, Q. *et al.* ATL3 Is a Tubular ER-Phagy Receptor for GABARAP-Mediated Selective Autophagy. *Current Biology* **29**, 846-855.e6 (2019).

10. Chino, H., Hatta, T., Natsume, T. & Mizushima, N. Intrinsically Disordered Protein TEX264 Mediates ER-phagy. *Molecular Cell* **74**, 909-921.e6 (2019).

11. Reggio, A. *et al.* Role of FAM134 paralogues in endoplasmic reticulum remodeling, ER phagy, and Collagen quality control. *EMBO Rep* **22**, (2021).

12. Bhaskara, R. M. *et al.* Curvature induction and membrane remodeling by FAM134B reticulon homology domain assist selective ER-phagy. *Nature Communications* **10**, (2019).

13. Jiang, X. *et al.* FAM 134B oligomerization drives endoplasmic reticulum membrane scission for ER phagy . *The EMBO Journal* **39**, (2020).

14. Alao, J. P., Legon, L. & Rallis, C. Crosstalk between the mtor and dna damage response pathways in fission yeast. *Cells* vol. 10 1–11 Preprint at https://doi.org/10.3390/cells10020305 (2021).

15. 1537.full.

16. Nassal, D., Gratz, D. & Hund, T. J. Challenges and opportunities for therapeutic targeting of calmodulin kinase II in heart. *Frontiers in Pharmacology* vol. 11 Preprint at https://doi.org/10.3389/fphar.2020.00035 (2020).

17. Gnad, F., Gunawardena, J. & Mann, M. PHOSIDA 2011: The posttranslational modification database. *Nucleic Acids Research* **39**, (2011).

18. Mochida, K. *et al.* Super-assembly of ER-phagy receptor Atg40 induces local ER remodeling at contacts with forming autophagosomal membranes. *Nature Communications* **11**, (2020).

19. Sauer, M. & Heilemann, M. Single-Molecule Localization Microscopy in Eukaryotes. *Chemical Reviews* vol. 117 7478–7509 Preprint at https://doi.org/10.1021/acs.chemrev.6b00667 (2017).

20. Roffey, S. E. & Litchfield, D. W. CK2 regulation: Perspectives in 2021. *Biomedicines* vol. 9 Preprint at https://doi.org/10.3390/biomedicines9101361 (2021).

21. Sanz-Clemente, A., Gray, J. A., Ogilvie, K. A., Nicoll, R. A. & Roche, K. W. Activated CaMKII Couples GluN2B and Casein Kinase 2 to Control Synaptic NMDA Receptors. *Cell Reports* **3**, 607–614 (2013).

22. Mochida, K. *et al.* Super-assembly of ER-phagy receptor Atg40 induces local ER remodeling at contacts with forming autophagosomal membranes. *Nature Communications* **11**, (2020).

23. Gordon, W. R. *et al.* Effects of S1 cleavage on the structure, surface export, and signaling activity of human Notch1 and Notch2. *PLoS ONE* **4**, (2009).

24. Edelstein, A. D. *et al.* Advanced methods of microscope control using μManager software. *Journal of Biological Methods* **1**, e10 (2014).

25. Schnitzbauer, J., Strauss, M. T., Schlichthaerle, T., Schueder, F. & Jungmann, R. Super-resolution microscopy with DNA-PAINT. *Nature Protocols* **12**, 1198–1228 (2017).

26. Descloux, A., Grußmayer, K. S. & Radenovic, A. Parameter-free image resolution estimation based on decorrelation analysis. *Nature Methods* **16**, 918–924 (2019).

27. Malkusch, S. & Heilemann, M. Extracting quantitative information from single-molecule super-resolution imaging data with LAMA - LocAlization Microscopy Analyzer. *Scientific Reports* **6**, (2016).

28. Ester, M., Kriegel, H.-P., Sander, J. & Xu, X. *A Density-Based Algorithm for Discovering Clusters in Large Spatial Databases with Noise*. www.aaai.org (1996).

29. el Beheiry, M. & Dahan, M. ViSP: Representing single-particle localizations in three dimensions. *Nature Methods* vol. 10 689–690 Preprint at https://doi.org/10.1038/nmeth.2566 (2013).

30. Perez-Riverol Y, Bai J, Bandla C, Hewapathirana S, García-Seisdedos D, Kamatchinathan S, Kundu D, Prakash A, Frericks-Zipper A, Eisenacher M, Walzer M, Wang S, Brazma A, Vizcaíno JA. The PRIDE database resources in 2022: A Hub for mass spectrometry-based proteomics evidences. *Nucleic Acids Res 50*(D1):D543-D552 (2022).

Figure legends

Figure 1. Chemical screen to identify kinases involved FAM134B- and FAM134C-driven ERphagy

(**A**) Schematic representation of the ERphagy flux assay using U2OS cells constitutively expressing the ssRFP-GFP-KDEL reporter and in addition overexpressing FAM134B (FAM134B) or FAM134C (FAM134C) in a doxycycline (DOX) inducible manner. Cells carrying the empty overexpression vector are used as control cells (CTRL). ERphagy flux is represented by the red/green (RFP/GFP) ratio of the total integrated fluorescent intensities. Higher values indicate higher ERphagy flux. au= arbitrary unit (**B**) ERphay flux analysis under basal (DMSO) and Torin1-induced conditions in the absence and presence of FAM134B/C overexpression. Differences in the ERphagy flux of CTRL and FAM134B/C overexpressing cells serve as the screening window for (**C**) to identify kinases involved in FAM134B/C-driven ERphagy upon Torin1 treatment. n=3, error bars=±STDV, [au]: arbitrary unit. (**C**) Heatmap of an ERphagy flux screen of appx. 100 probe and probe-like kinase inhibitors and available negative control compounds (1µM final concentration) in the presence of 250nM Torin1, using U2OS cells described in (**A**). Total integrated fluorescent intensities (RFP/red and GFP/green) were monitored in the IncuCyte®S3 over a time course of 48 h. Data points represent the averaged red/green ratio of three images comprising >150 cells and taken from three independent wells (here defined as technical replicates). Included

control values: DMSO = complete suppression; Torin1 = no effect. This experiment was performed once and validation of positive hits in Fig. 2A-B was performed at least three times (n=3).

Figure 2. mTOR inhibition triggers phosphorylation of FAM134B and FAM134C by CK2

(**A and B**) Validation of kinase screening HITs counteracting the effect of Torin1 in FAM134B- (**A**) or FAM134C- (**B**) overexpressing cells. Left panels: Analytic representation of FAM134B or FAM134C - induced ERphagy changes upon treatment with a dilution series of selected compounds (SGC-CK2-1 (CK2i), VE-822 (ATRi), KU-60019/KU-55933 (ATMi), CHIR-124 (Chk1i) and MK-2206 2HCL (AKTi)) ranging from 0,01 µM to 4 µM combined with Torin1 treatment. DMSO was set to represent 100% inhibition of FAM134B- and FAM134C-induced ERphagy while Torin1 represents 0%. Averaged RFP/GFP ratio measured in response to HIT compound treatments was normalized at each time point to the averaged RFP/GFP ratio of DMSO and Torin1. Right panels: Growth of U2OS cells overexpressing FAM134B or FAM134C treated with indicated compounds and concentrations and recorded over a time period of 48h (data from 3 time points are shown in the bar graphs). error bars=±STDV of technical replicates (n=3). This experiment was repeated twice with similar results. (**C**) Schematic representation of FAM134B/C proteins highlighting the reticulon homology domain (RHD; white) comprising two transmembrane domains (TM1/2 and TM3/4; blue) flanked by membrane associated linker regions (green), the conserved LC3 interacting motif (LIR), as well as sites of dynamic phosphorylation events.

(**D**) Representative image of an Co-IP experiment of HA-FAM134B (left) or HA-FAM134C (right) (HA; bait) and endogenous CK2 (prey) in lysates of U2OS cells overexpressing indicated HA-FAM134 proteins and grown under basal, 250 nM Torin1 or 250 nM Torin1 + 1 µM CK2 inhibitor conditions. 200 ng/ml Bafilomycin A1 was added 3 h prior cell lysis (n=2).

Figure 3. FAM134B & FAM134C phosphorylation by CK2 is perquisite for their ubiquitination and Torin1-dependant ERphagy induction

(**A**) FAM134B & FAM134C are ubiquitinated under basal conditions. Schematic representation of Tandem Ubiquitin Binding Entities pulldown assay (TUBE2) performed in U2OS cells overexpressing FAM134B or FAM134C in DOX-dependent manner which were subjected to different conditions to then purify mono- and poly-ubiquitinated FAM134s proteins. (**B**) Representative western blot showing enrichment for poly ubiquitinated FAM134 proteins using TUBE2 assay. U2OS cells overexpressing FAM134B or FAM134C proteins were treated or not with 200 ng/ml Bafilomycin A1 3 h prior cell lysis and pull-down experiment. Anti-HA antibody was used to detect HA-tagged FAM134B and FAM134C as well as ubiquitinated species (n=2). (**C**) Exemplary pictures of U2OS cells overexpressing FAM134B or FAM134C and stably expressing KDEL reporter and exposed to indicated conditions. Pictures were acquired using the IncuCyte® S3 (10x) and show the overlaid GFP and RFP signal from DMSO, Torin1 and Torin1 + E1 inhibitor treated cells at time point 24 h. (**D**) Quantitative representation of ERphagy flux essay performed in (**C**) analyzing changes over time in FAM134B- (left panel) and FAM134C-induced ERphagy (right panel) upon treatment with E1 inhibitor dilution series in combination with 250 nM Torin1. Each data point represents average of three technical replicates collected from three individual wells. This experiment was repeated once with similar results. (**E**) Ubiquitination of FAM134B and FAM134C is dependent on their phosphorylation via CK2. Representative western blot (upper panel) and corresponding quantification (lower panel) of Tube2 assay in U2OS cells overexpressing FAM134B (left panel) or FAM134C (right panel) subjected for 6h to the indicated conditions prior cell lysis. Pull down of ubiquitinated entities was performed as in Figure 3A. anti-HA antibody was used to detect HA-tagged FAM134B and FAM134C and ubiquitinated species. Anti-HA signal from inputs was used as reference for ratio calculation.

(n=2) (**F**) Representative western blot of the bimolecular complementation affinity purification assay (BiCAP) showing ubiquitination status of FAM134B (left panel) and FAM134C (right panel) dimers. GFP trap pulldown was performed to immuno-precipitate reconstituted GFP representing FAM134B or FAM134C dimers. Anti-FAM134B or anti-FAM134C antibodies were used to detect endogenous proteins while anti-Ub was used to detect ubiquitination. (n=2)

Figure 4. Phosphorylation of FAM134B and FAM134C proteins impacts their clustering

(**A**) Schematic representation of sample preparation for exchange DNA-PAINT experiment performed on U2OS overexpressing FAM134B & FAM134C upon 12h DOX induction. Cells were grown under basal, 250 nM Torin1 or 250 nM Torin1 + 1 µM CK2 inhibitor conditions. 200 ng/ml Bafilomycin A1 was added 3hrs prior to sample preparation. (**B**) Super-resolved DNA-PAINT images showing HA-FAM134B (left panel) and HA-FAM134C (right panel) labeling in U2OS cells treated as described in Fig 4.A. Localization of single molecules and reconstruction of clusters are annotated in the region of interest. Scale bars: 10 and 1 µm. (**C-D**) Quantitative analysis of FAM134B (**C**) and FAM134C (**D**) nanocluster diameters in indicated conditions (250 nM Torin1 or 250 nM Torin1 + 1 µM CK2 inhibitor). Quantification was performed via DBSCAN clustering algorithm 3 and distribution of clusters was assessed in WT FAM134B- and FAM134C-overexpressing U2OS cells and their respective mutants (FAM134B S149, 151 153A and FAM134C S258A) (**E-J**). Comparative analysis of the relative protein density for FAM134B VS. mutant (**E-G**) and FAM134C VS mutant (**H-J**). Frequency of transient binding events (localization) per nanoscale cluster was analyzed under basal, 250 nM Torin1 or 250 nM Torin1 + 1 µM CK2 inhibitor conditions. Statistical analysis: FAM134B and FAM134C nanocluster diameter were tested for normal distribution via Shapiro-Wilk normality test and statistical significance via non-parametric Mann-Whitney U-test. For further details see M&M.

Figure 5. Model of the study: FAM134B- and FAM134C- dependent ERphagy induction is regulated by early interdependent posttranslational modification (PTM) events.

Induction of ER stress via mTOR inhibition triggers phosphorylation of FAM134B and FAM134C which primes for their ubiquitination. Both PTM are essential for the oligomerization process of both FAM134s and control the size and density of the clustering events leading to ER budding and ERphagy induction.

Supplementary figure legends

Supplementary figure 1. Identification of kinases involved in FAM134B/C and mTOR-regulated ERphagy

(**A**) Heatmap indicating the cell confluence over time (% of covered area) corresponding to Figure 1C. (**B**) Schematic workflow for data transformation to calculate the relative reduction of Torin1-induced ERphagy flux. Cpd: compounds. (**C**) Relative reduction of ERphagy flux caused by HIT compounds counteracting Torin1-induced FAM134B- and FAM134C-driven ERphagy, respectively. HITs were defined as compounds causing >20% relative reduction in ERphagy flux over a minimum time period of 12h. (**D**) Relative reduction of FAM134B-driven ERphagy flux upon CaMKII inhibition. Data points represent cell confluence (Supplementary Fig. 1A) or averaged red/green ratio (Supplementary Fig. 1C-D) of three images comprising >150 cells and taken from three independent wells. These experiments were performed 3 times with similar results.

Supplementary figure 2. Validation of chemical kinase screen and identification of CK2 as kinase regulating FAM134B- and FAM134C-dependant ERphagy

(**A**) Sample pictures of U2OS cells overexpressing FAM134B or FAM134C and stably expressing KDEL reporter. Pictures were acquired by the IncuCyte® S3 (10x) and show the overlaid GFP and RFP signal from annotated conditions at time point 48 h. (**B**) Impact of selected HITs on ERphagy flux and cell growth in U2OS control cells. U2OS cells stably expressing KDEL reporter were subjected to a dilution series of selected compound HITs (SGC-CK2-1 (CK2i), VE-822 (ATRi), KU-60019 (ATMi), CHIR-124 (Chk1i) and MK-2206 2HCL (AKTi)) ranging from 0,01 µM to 4 µM combined with Torin1 treatment. Outcome on ERphagy flux (left panel) and cell growth (right panel) was recorded over 48h. error bars=±STDV of technical replicates (n=3). This experiment was repeated twice with similar results. (**C**) Predicted kinases phosphorylating identified serines of FAM134B and FAM134C proteins using motif matcher tool PHOSIDA. (**D**) Representative image of colloidal blue-stained gel of immunoprecipitated HA-FAM134C showing higher-order signals of the protein (n=2).

Supplementary figure 3.

(**A**) List of selected HITs from the ERphagy screening performed in Figure 1C showing compounds with an effect on FAM134B (left panel) or FAM134C (right panel) activities. (**B**) Multiple sequence alignment of FAM134B and FAM134C showing the conservation level of dynamic phosphorylation sites presented in Figure 1C. (**C**) Representative scheme outlining the principle behind BiCAP assay using the Venus split system coupled with GFP trap pulldown assay.

Supplementary figure 4. FAM134B and FAM134C cluster analysis and binding to LC3B

(**A-F**) Comparative analysis of subdivided nanoscale clusters of small (30-90 nm), medium (90-150 nm) and large clusters dimeters (> 150 nm) showing the plotted relative frequency distribution of localizations per cluster comparing DMSO, Torin1 and Torin1+CK2i

conditions in FAM134B (**A-C**) and FAM134C (**D-F**). Statistical analysis: FAM134B and FAM134C nanocluster diameter were tested for normal distribution via Shapiro-Wilk normality test and statistical significance via non-parametric Mann-Whitney U-test. For further details see M&M.

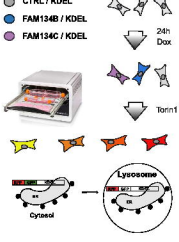
CTRL / KDEL
FAM134B / KDEL
FAM134C / KDEL
24h
Dox
Torin1
Lysosome
Cytosol

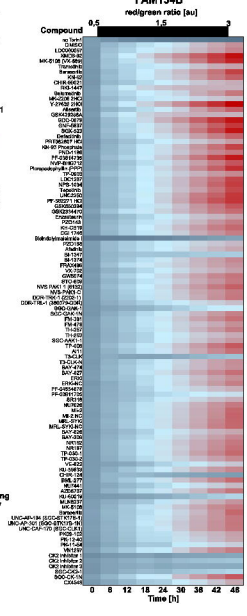
FAM134B
red/green ratio [au]
Compound
Time [h]

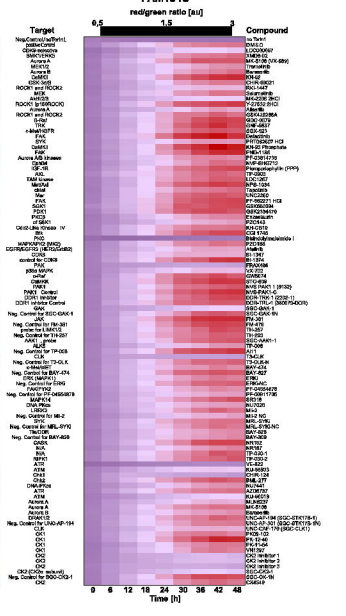
FAM134C
red/green ratio [au]
Target
Compound
Time [h]

B

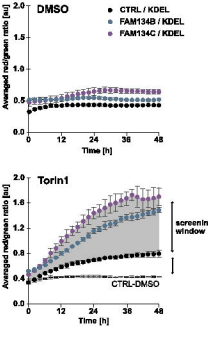
DMSO
CTRL / KDEL
FAM134B / KDEL
FAM134C / KDEL
Averaged red/green ratio [au]
Time [h]
Torin1
screening window
CTRL-DMSO

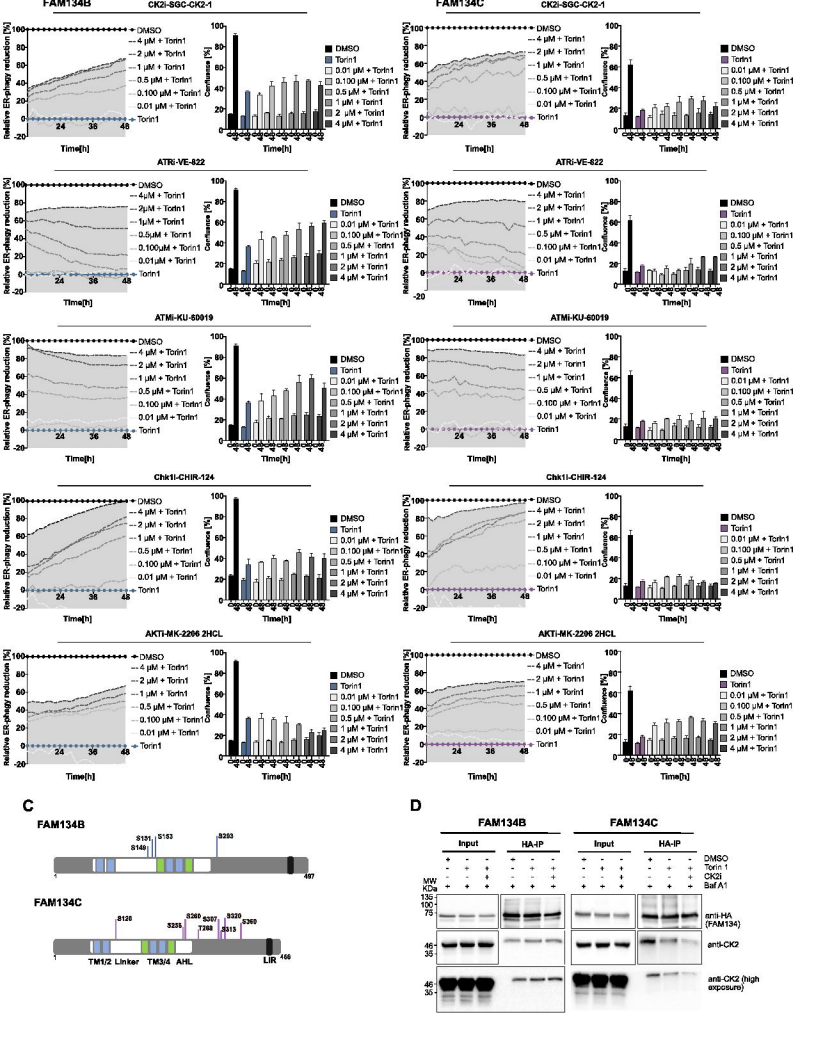
FAM134B
CK2i-SGC-CK2-1
FAM134C
CK2i-SGC-CK2-1
ATRi-VE-822
ATRi-VE-822
ATMi-KU-60019
ATMi-KU-60019
Chk1i-CHIR-124
Chk1i-CHIR-124
AKTi-MK-2206 2HCL
AKTi-MK-2206 2HCL
Relative ER-phagy reduction [%]
Confluence [%]
Time[h]
DMSO
Torin1
0.01 μM + Torin1
0.100 μM + Torin1
0.5 μM + Torin1
1 μM + Torin1
2 μM + Torin1
4 μM + Torin1
C
FAM134B
S131
S153
S140
S203
1
497
FAM134C
S128
S235
S260
S307
T268
S320
S313
S360
1
TM1/2 Linker
TM3/4
AHL
LIR
466
D
FAM134B
FAM134C
Input
HA-IP
DMSO
Torin 1
CK2i
Baf A1
MW
KDa
anti-HA (FAM134)
anti-CK2
anti-CK2 (high exposure)

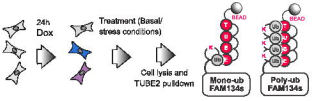
24h
Dox
Treatment (Basal/
stress conditions)
Cell lysis and
TUBE2 pulldown
HEAD
Mono-ub
FAM134s
Poly-ub
FAM134s

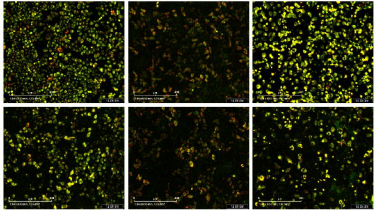
FAM134C
FAM134B

B

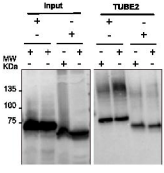
Input
TUBE2
HA-FAM134B
HA-FAM134C
BafA1
DMSO
MW
KDa
135
100
75
anti-HA
(FAM134)

D

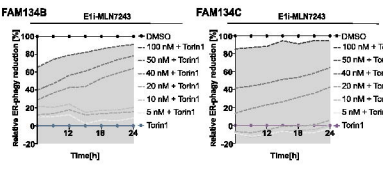
FAM134B
E1i-MLN7243
FAM134C
E1i-MLN7243
DMSO
100 nM + Torin1
50 nM + Torin1
40 nM + Torin1
20 nM + Torin1
10 nM + Torin1
5 nM + Torin1
Torin1
relative ER-phagy reduction [%]
Time[h]

E

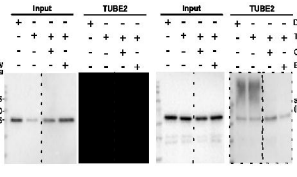
FAM134B
FAM134C
Input
TUBE2
DMSO
Torin1
CK2i
E1i
MW
KDa
135
100
75
anti-HA
(FAM134)

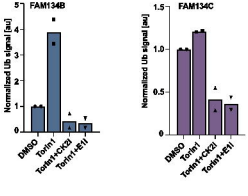
FAM134B
FAM134C
Normalized Ub signal [au]
DMSO
Torin1
Torin1+CK2i
Torin1+E1i

F

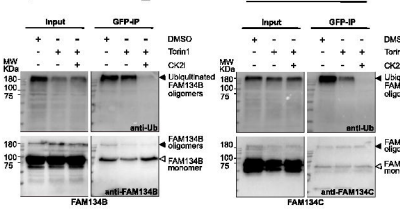
FAM134B
FAM134C
Input
GFP-IP
DMSO
Torin1
CK2i
MW
KDa
180
100
75
Ubiquitinated
FAM134B
oligomers
Ubiquitinated
FAM134C
oligomers
anti-Ub
FAM134B
oligomers
FAM134B
monomer
FAM134C
oligomers
FAM134C
monomer
anti-FAM134B
anti-FAM134C

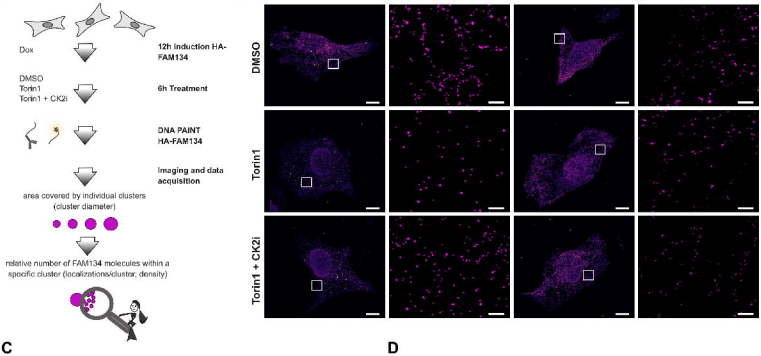
Dox
12h induction HA-FAM134
DMSO
Torin1
Torin1 + CK2i
6h Treatment
DNA PAINT HA-FAM134
Imaging and data acquisition
area covered by individual clusters (cluster diameter)
relative number of FAM134 molecules within a specific cluster (localizations/cluster; density)
DMSO
Torin1
Torin1 + CK2i

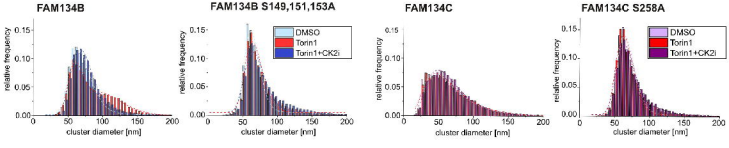
C
FAM134B
FAM134B S149,151,153A
D
FAM134C
FAM134C S258A
DMSO
Torin1
Torin1+CK2i
relative frequency
cluster diameter [nm]

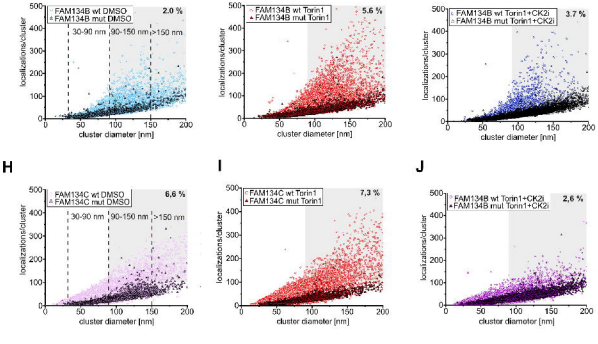
E
FAM134B wt DMSO
FAM134B mut DMSO
30-90 nm
90-150 nm
>150 nm
2.0 %
F
FAM134B wt Torin1
FAM134B mut Torin1
5.6 %
G
FAM134B wt Torin1+CK2i
FAM134B mut Torin1+CK2i
3.7 %
H
FAM134C wt DMSO
FAM134C mut DMSO
6.6 %
I
FAM134C wt Torin1
FAM134C mut Torin1
7.3 %
J
FAM134B wt Torin1+CK2i
FAM134B mut Torin1+CK2i
2.6 %
localizations/cluster
cluster diameter [nm]

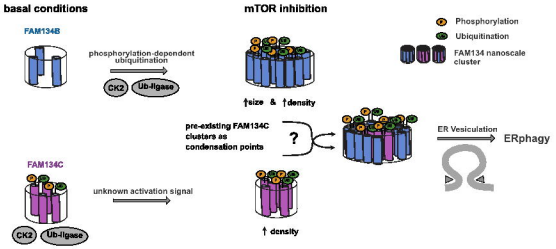
basal conditions
mTOR inhibition
FAM134B
phosphorylation-dependent ubiquitination
CK2
Ub-ligase
↑size & ↑density
Phosphorylation
Ubiquitination
FAM134 nanoscale cluster
pre-existing FAM134C clusters as condensation points
?
ER Vesiculation
ERphagy
FAM134C
unknown activation signal
CK2
Ub-ligase
↑ density

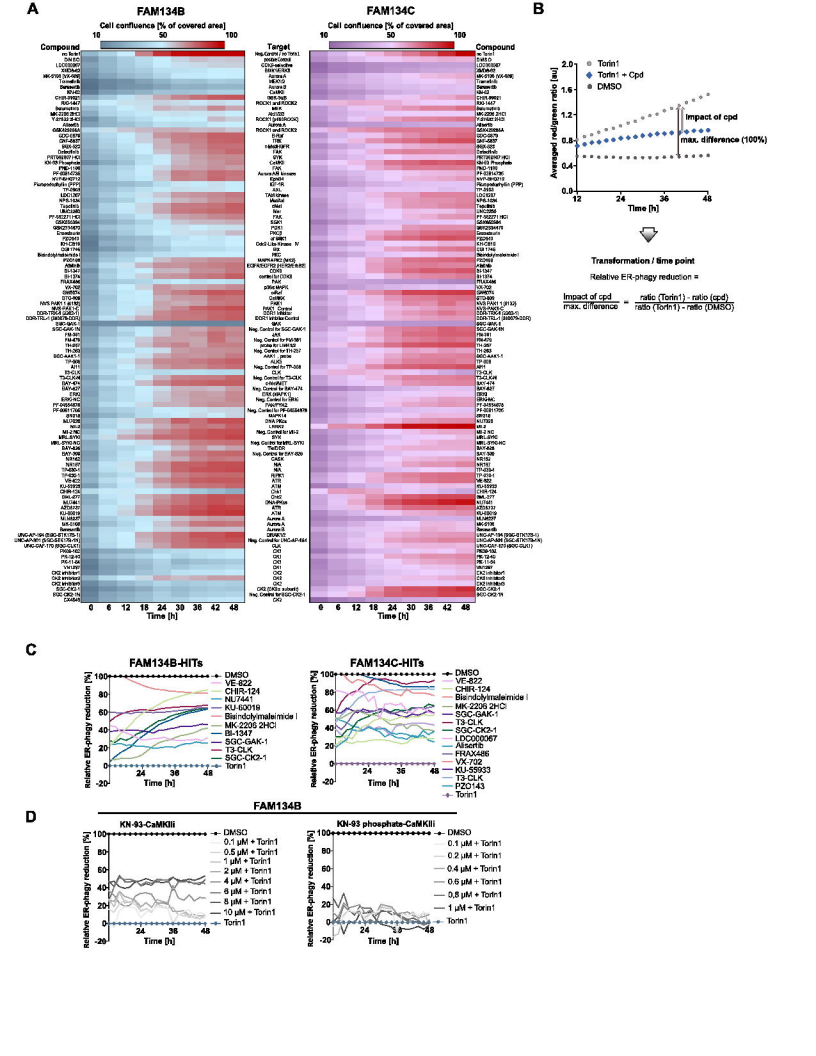
A
FAM134B
FAM134C
Cell confluence [% of covered area]
Compound
Target
Time [h]
B
Torin1
Torin1 + Cpd
DMSO
Impact of cpd
max. difference (100%)
Averaged red/green ratio [au]
Time [h]
Transformation / time point
Relative ER-phagy reduction =
Impact of cpd / max. difference = ratio (Torin1) - ratio (cpd) / ratio (Torin1) - ratio (DMSO)
C
FAM134B-HITs
FAM134C-HITs
Relative ER-phagy reduction [%]
Time [h]
DMSO
VE-822
CHIR-124
NL7441
KU-60019
Bisindolylmaleimide I
MK-2206 2HCl
BI-1347
SGC-GAK-1
T3-CLK
SGC-CK2-1
Torin1
D
FAM134B
KN-93-CaMKIII
KN-93 phosphate-CaMKIII
0.1 µM + Torin1
0.5 µM + Torin1
1 µM + Torin1
2 µM + Torin1
4 µM + Torin1
6 µM + Torin1
8 µM + Torin1
10 µM + Torin1
Torin1
0.2 µM + Torin1
0.4 µM + Torin1
0.6 µM + Torin1
0.8 µM + Torin1
1 µM + Torin1

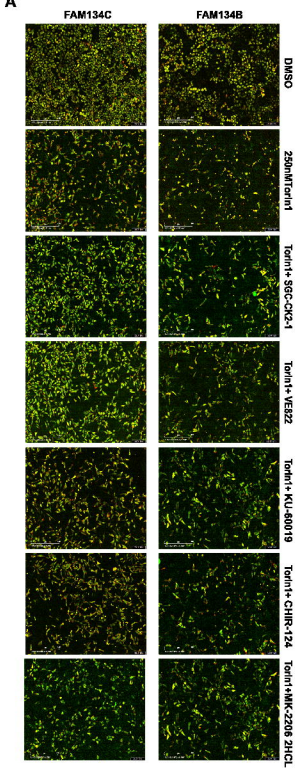

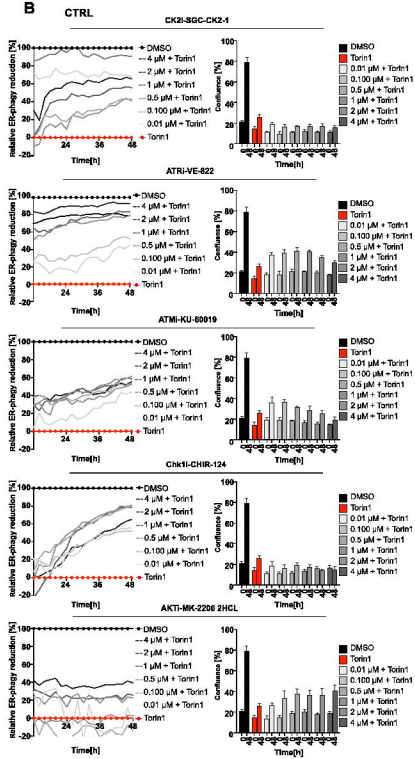

C

Protein	Serine #	Predicted kinase (PHOSIDA)
FAM134B	S149	**CK2** (S/T-X-X-E) GSK3 (S-X-X-X-S)
	S151	CAMK2 (R-X-X-S/T) **CK2** (S-X-X-S/T)
	S153	CK1 (S/T-X-X-X-S) NEK6 (L-X-X-S/T)
	S293	Aurora (R/K-X-X-S/T-I/L/V)
FAM134C	S126	**CK2** (S/T-X-X-E) CAMK2 (R-X-X-S/T, R-X-X-S/T-V)
	S258	**CK2** (S/T-X-X-E)
	S260	**CK2** (S/T-X-X-E)
	S288	**CK2** (S/T-X-X-E)
	S307	**CK2** (S/T-X-X-E)
	S313	N/A
	S320	**CK2** (S/T-X-X-E)
	S350	N/A

D

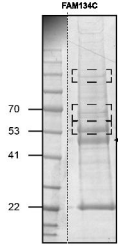

A

FAM134B-HIT list

Selected Hits with >20% Torin-1 Induced ER/phagy Inhibition	Targetad kinase
SGC-CK2-1	Catalytic subunits of CK2: CKα (CSNK2A1) and CKα' (CSNK2A2)
VE-822	ATR
KU-55933	ATM
CHIR-124	Chk1
MK-2206 2HCl	Akt1/2/3
SGC-GAK1	GAK
T3-CLK I	CLK
Bisindolylmaleimide I	PKC inhibitor I
NU7441	DNA-PKCs
CHIR-99021	GSK-3α/β

FAM134C-HIT list

Selected Hits with >20% Torin-1 Induced ER/phagy Inhibition	Targetad kinase
SGC-CK2-1	Catalytic subunits of CK2: CKα (CSNK2A1) and CKα' (CSNK2A2)
VE-822	ATR
KU-55933	ATM
CHIR-124	Chk1
MK-2206 2HCl	Akt1/2/3
SGC-GAK1	GAK
T3-CLK I	CLK
Bisindolylmaleimide I	PKC inhibitor I
Aliseri b	Aurora A
VX-702	p38α MAPK
FRAX486	PAK
LDC000067	CDK9
RKI-1447	ROCK1 and ROCK2
PZC143	S6K1
Afatinib	EGFR/EGFR2 (HER2/Erb32)

B

FAM134B sequence alignment

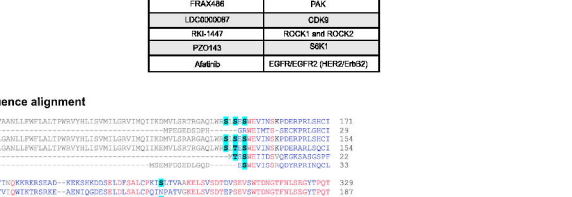

FAM134C sequence alignment

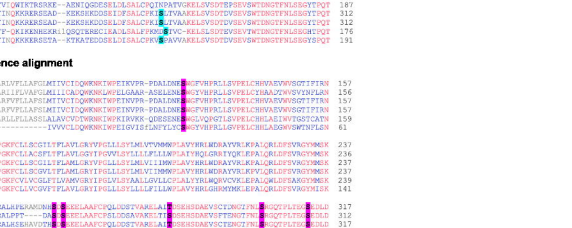

C

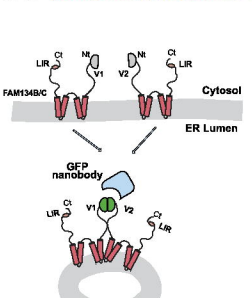

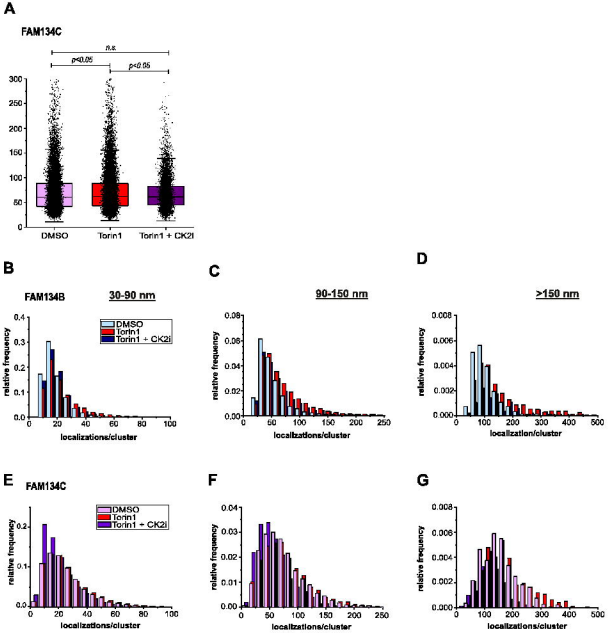
A
FAM134C
n.s.
p<0.05
p<2.55
DMSO
Torin1
Torin1 + CK2i
B
FAM134B
30-90 nm
C
90-150 nm
D
>150 nm
relative frequency
localizations/cluster
E
FAM134C
F
G